Supplemental Figure Legends

Supplementary Figure 1. miRs are differentially expressed during CD8 T cell differentiation in acute and chronic infection.

C57/BL6 mice were infected with either LCMV Armstrong ("acute") or LCMV clone 13 ("chronic"). At d8 and at d30 p.i. LCMV D^b gp-33 specific CD8 T cells were purified from spleens and their miR profile was examined using Affymetrix microRNA 2.0 array. As a control, CD8 T cells from naïve mice were purified ("T_N").

(*A*) Mean expression level and STDV for all the differentially expressed miRs (DEM; FDR<0.05) between T_N, T_{EFF} and T_{MEM}.

(*D*) Mean expression level and STDV f(*B* - *C*) Venn diagrams showing the differentially expressed miRs (DEM; FDR<0.05) between T_N, T_{EFF} and T_{MEM} (*B*) and between T_N, T_{EE} and T_{EX} (*C*). Red represents upregulation in the first group of the pairwise comparison; blue represents downregulation in the first group of the pairwise comparison.

or all the differentially expressed miRs (DEM; FDR<0.05) between T_N, T_{EE} and T_{EX}.

(*E*) Venn diagram showing DEM (FDR<0.05) between T_{EFF} vs T_{EE} and T_{MEM} vs T_{EX}. Red represents upregulation in the first group of the pairwise comparison.

(*F*) MiR-29a expression levels and fold-cahnges in T_N, T_{EFF}, T_{MEM}, T_{EE} and T_{EX}.

Supplementary Figure 2. Key transcriptional pathways are implicated in miR differential regulation between acute and chronic infection.

(*A*-*C*) C57/BL6 mice were infected with LCMV Armstrong or clone 13. At d8 and at d30 p.i. LCMV D^b gp-33 specific CD8 T cells were purified from spleens and their miR profile was examined as in Figure 1. (*A*) A network of miRs and their predicted targets that were DE between acute and chronic infection at d8 p.i. was constructed using the filtered miR-mRNA target list from Figure 2*B*. (*B*) Intracellular staining for Eomes in CD44+ CD8 T cells from splenocytes of mice infected with LCMV Armstrong (grey filled histogram) or LCMV clone 13 (black open histogram) at d30 p.i. (*C*) Upstream regulators of DEM and target DEG from the filtered miR-mRNA target list from Figure 2*B* at d8 and at d30 p.i. (*D*) P14 cells were transduced with control (empty) RV or miR-29a RV. Transduction efficiency was measured by fow cytometry at 24 hrs post transduction. Mean % of VEX+ cells out of total P14 ± SEM is shown (top black: control RV; bottom red: miR-29a OE RV). (*E*) CD45.1+ P14 CD8 T cells were transduced with either control-VEX RV (ctrl) or miR-29a OE RV (miR) and adoptively transferred to CD45.2+ recipient mice that were infected with LCMV clone 13 at 24 hrs earlier. Frequency and phenotype of donor VEX+ P14 cells in spleens at d8 p.i. is shown.

(*F*-*G*) CD45.1+ P14 CD8 T cells were transduced with either scrambled-GFP RV or miR-29a OE-GFP RV (miR) and adoptively transferred to CD45.2+ recipient mice that were infected with LCMV clone 13 at 24 hrs earlier. At d30 p.i. the phenotype of the transferred and transduced cells was analyzed by flow cytometry. (*F*) FACS plots are gated on total P14 CD45.1+ cells. (*G*) FACS plots are gated on GFP+ P14 cells. Each data point represents an individual mouse. *P* values calculated with Mann-Whitney test.

Supplementary Figure 3. The miR-29a effects on T_{EX} differentiation are intrinsic to CD8 T cells and result in a T_{MEM}-like transcriptional profile.

(*A-B*) CD45.1+ P14 CD8 T cells were transduced with either control-VEX RV (ctrl) or miR-29a OE-VEX RV (miR) and adoptively transferred to CD45.2+ recipient mice that were infected with LCMV clone 13 at 24 hrs earlier. (*A*) Viral loads for LCMV were analyzed in the serum at d30 p.i. using plaque assay. (*B*) Expression of surface markers was analyzed on non-transduced (VEX negative) P14 cells at d30 p.i. in spleens.

(*C*) 10^6 CD8 T cells purified from splenocytes from CD45.2+ miR-29ab1$^{fl/fl}$ CD4 Cre^{+} ("miR-29a ko") and littermate control wild-type (wt) mice were transferred to wild-type CD45.1 recipient mice that were infected with LCMV clone 13 at 24 hrs later. Donor wt or ko CD8 T cells were analyzed at d13 p.i. FACS plots are gated on donor CD45.2+ cells. Each data point represents an individual mouse.

(*D*) CD8 T cells were purified from spleens of WT mice and transduced with empty RV or miR-29a-OE RV (both expressing VEX as a reporter) and with a 3'UTR sensor GFP reporter RV (33) containing either *Gadph* 3'UTR or *Eomes* 3'UTR. 24h later, GFP expression was analyzed by flow cytometry. FACS plots are gated on VEX+ CD8 T cells.

(*E*) miR-29a-OE VEX+ P14 and control VEX+ P14 cells were sorted from spleens at d30 p.i. and quantitative RT-PCR was performed.

(*F-I*) RNASeq was performed using control or miR-29a-OE VEX+ P14 from d30 p.i. with LCMV clone 13 (as described in Figure 3). (*F*) GSEA for a geneset of predicted miR-29a targets (from MSigDB). (G) Leading edge genes significantly enriched in control vs miR-29a OE cells (from Fig. S3*E*). (*H*) GSEA for a geneset of T_{EFF} vs T_{MEM} (from MSigDB). (*I*) GSEA for a geneset of genes upregulated upon miR-155-OE (from Stelekati et al., 2018). Table shows leading edge genes significantly enriched in control vs miR-29a OE cells.

Supplementary Figure 4. Fos and Tox OE antagonize the effects of miR-29 OE and miR-29a OE enhances CD8 T cell responses during acute infection

(*A*) CD45.1+ P14 CD8 T cells were transduced with miR-29a-GFP RV and empty-VEX RV or Jun-VEX RV (OE Jun) or Fos-VEX RV (OE Fos) or Tox-VEX RV (OE Tox). P14 cells transduced with empty-GFP RV and empty-VEX RV served as negative control. 5 x 10^4 cells were adoptively transferred to CD45.2+ recipient mice that were infected with LCMV clone 13 at 24 hrs earlier. P14 cells transduced with both RV were identified as VEX+ GFP+ cells and analyzed at d14 p.i. FACS plots are gated on transferred CD45.1+ P14 cells. Histograms showing the phenotype of cells are gated on VEX+ GFP+ P14 cells. Each data point represents an individual mouse. Statistical significance was calculated using Kruskal-Wallis test with Dunn's multiple comparison post-test.

(*B-D*) CD45.1+ P14 CD8 T cells were transduced with either control-VEX RV (ctrl) or miR-29a OE-VEX RV (miR) and adoptively transferred to CD45.2+ recipient mice that were infected with LCMV Armstrong at 24 hrs earlier. (*B*) Expansion of transferred P14 cells at d35 p.i. in spleens. (*C*) Surface expression of CD127 and KLRG1 on VEX+ P14 cells (*D*) Cytokine production by VEX+ P14 cells after ex vivo 5hr re-stimulation with gp-33 peptide.

Supplementary Table 1. Differentially expressed transcripts with FDR<0.05 between ctrl and miR-29a-OE CD8 T cells.

P14 cells were transduced with miR-29-OE or control RV and adoptively transferred into congenically marked recipient mice as described in Fig. 3*A*. At d30 p.i., miR-29-OE and control VEX+ P14 cells were sorted by FACS and RNASeq was performed. Table shows transcripts differentially expressed between miR-29-OE and control VEX+ P14 cells with FDR<0.05.

Supplementary Table 2. Pathway analysis reveals a role for miR-29a in regulating ribosomal pathways.

RNASeq analysis was performed in miR-29-OE and control P14 CD8 T cells exposed to clone 13 infection for 30 d, as described in Fig. 3. GSEA was performed using the database MSigDB. Table shows pathways from the GO Molecular Functions database enriched with FDR<0.05.

Supplementary Table 3. miR-29a abrogates the response to antigen signaling and inflammation.

RNASeq analysis was performed in miR-29-OE and control P14 CD8 T cells exposed to clone 13 infection for 30 d, as described in Fig. 3. GSEA was performed using the database MSigDB. Table shows pathways from the Hallmark database enriched in control vs miR-29-OE P14 CD8 T cells (with FDR<0.05).

Supplementary Table 4. GSEA analysis implicates major transcription factors regulation by miR-29a.

RNASeq analysis was performed in miR-29-OE and control P14 CD8 T cells exposed to clone 13 infection for 30 d, as described in Fig. 3. GSEA was performed using the database MSigDB. Table shows pathways from the PID database enriched in control vs miR-29-OE P14 CD8 T cells (with FDR<0.05).

•

Figure S1

A

	TN		TEFF		TMEM	
microRNA	mean	STDV	mean	STDV	mean	STDV
mmu-let-7b	10.84	0.50	6.87	0.54	10.29	0.10
mmu-let-7c	10.88	0.54	7.51	0.55	10.63	0.11
mmu-miR-130b	3.76	0.94	6.01	0.89	4.70	1.16
mmu-miR-139-5p	5.89	0.80	3.11	0.75	7.11	0.32
mmu-miR-140-star	6.24	0.71	4.82	1.31	7.51	0.28
mmu-miR-146a	3.79	1.16	8.77	1.06	10.26	0.72
mmu-miR-155	5.56	0.75	8.03	0.70	8.59	0.80
mmu-miR-181a	7.79	0.58	3.68	0.36	4.23	1.24
mmu-miR-182	2.51	0.69	7.54	0.83	5.39	1.78
mmu-miR-183	2.11	0.58	5.38	1.06	2.84	1.03
mmu-miR-21	2.44	0.63	5.38	2.25	6.00	1.91
mmu-miR-2137	4.34	1.41	7.89	1.18	7.13	0.53
mmu-miR-221	3.42	0.67	4.91	1.47	5.95	0.87
mmu-miR-222	2.87	0.57	4.79	1.25	4.75	1.37
mmu-miR-26a	9.43	0.31	7.16	1.15	10.18	0.57
mmu-miR-27b	4.54	0.72	6.58	1.43	6.78	1.39
mmu-miR-29a	6.84	0.36	5.46	1.71	8.97	0.75
mmu-miR-31	2.64	0.63	6.69	0.85	7.59	0.65
mmu-miR-320	5.98	0.72	3.50	0.74	5.44	0.39
mmu-miR-342-3p	9.84	0.26	6.90	0.41	9.47	0.31
mmu-miR-342-5p	6.79	0.45	3.08	0.30	4.62	1.04
mmu-miR-378	6.85	0.49	4.19	1.09	7.27	0.44

B

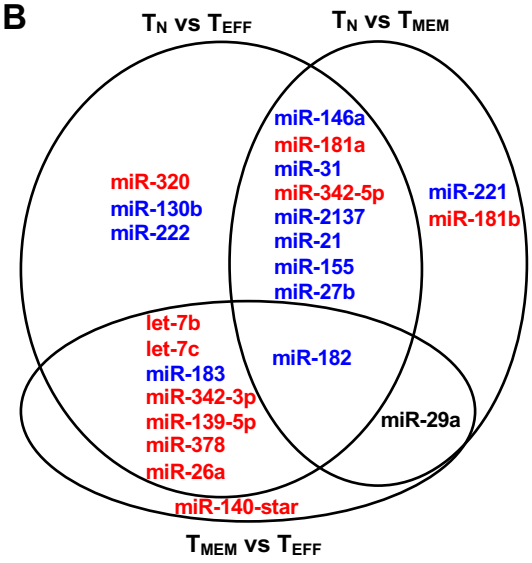

C

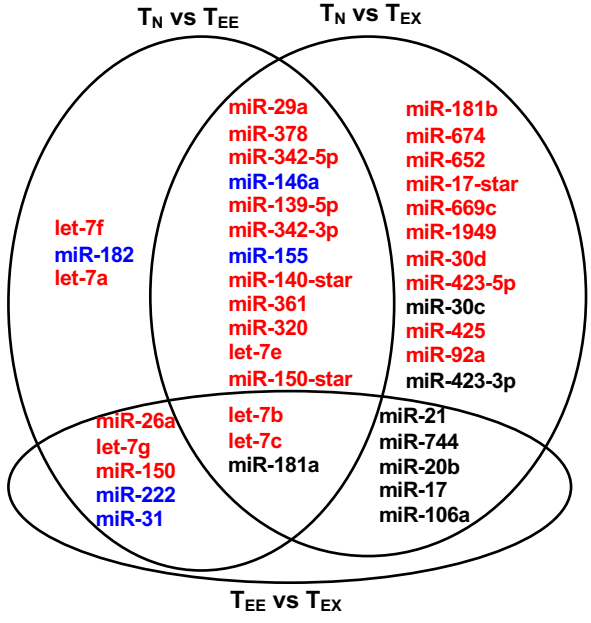

D

	TN		TEE		TEX	
	mean	STDV	mean	STDV	mean	STDV
mmu-let-7a	9.81	0.49	7.45	0.41	9.10	0.97
mmu-let-7b	10.84	0.50	6.07	0.20	8.40	0.74
mmu-let-7c	10.88	0.54	6.23	0.32	8.85	0.71
mmu-let-7e	4.40	1.34	2.31	0.40	2.23	1.91
mmu-let-7f	6.49	0.52	3.61	0.61	5.04	2.38
mmu-let-7g	7.23	0.44	4.35	0.59	6.50	1.55
mmu-miR-106a	5.46	0.47	6.09	0.80	3.45	2.33
mmu-miR-139-5p	5.89	0.80	2.32	0.36	3.34	2.44
mmu-miR-140-star	6.24	0.71	3.51	0.48	4.09	2.81
mmu-miR-146a	3.79	1.16	7.39	0.88	8.41	0.99
mmu-miR-150-star	5.04	1.18	3.04	0.62	2.85	2.05
mmu-miR-150	11.82	0.30	9.12	0.37	11.16	0.79
mmu-miR-155	5.56	0.75	8.77	0.70	9.81	0.63
mmu-miR-17-star	4.25	1.29	2.84	0.34	1.90	1.38
mmu-miR-17	6.60	0.20	7.01	0.96	4.45	2.16
mmu-miR-181a	7.79	0.58	4.06	0.58	2.01	1.38
mmu-miR-181b	4.41	0.99	3.27	0.57	1.58	1.21
mmu-miR-182	2.51	0.69	5.03	1.24	3.56	2.51
mmu-miR-1949	4.27	0.81	3.87	0.54	2.09	1.35
mmu-miR-20a	5.52	0.40	5.60	0.86	3.76	2.42
mmu-miR-20b	5.40	0.51	5.23	0.97	3.18	2.40
mmu-miR-21	2.44	0.63	3.32	0.59	6.37	2.14
mmu-miR-222	2.87	0.57	5.07	0.58	2.86	2.24
mmu-miR-26a	9.43	0.31	5.48	0.90	8.28	1.03
mmu-miR-29a	6.84	0.36	3.08	0.58	4.64	3.19
mmu-miR-30d	4.64	0.77	2.92	0.89	2.50	2.22
mmu-miR-31	2.64	0.63	4.56	0.69	2.20	1.71
mmu-miR-320	5.98	0.72	3.64	0.67	2.95	2.04
mmu-miR-342-3p	9.84	0.26	6.36	0.75	6.01	2.39
mmu-miR-342-5p	6.79	0.45	3.18	0.97	2.25	1.50
mmu-miR-361	6.56	0.43	3.86	0.57	3.91	2.59
mmu-miR-378	6.85	0.49	3.22	0.08	3.36	2.74
mmu-miR-423-5p	3.90	1.22	3.14	1.02	1.80	1.17
mmu-miR-425	4.88	0.97	4.61	0.61	2.96	2.31
mmu-miR-652	6.35	0.72	4.96	0.97	3.80	2.73
mmu-miR-669c	3.93	1.54	2.40	0.54	1.62	1.18
mmu-miR-674	4.49	0.31	3.36	0.75	1.94	1.46
mmu-miR-744	4.34	1.04	4.31	0.60	2.05	1.32
mmu-miR-92a	9.90	0.54	8.31	0.38	7.98	0.84

E

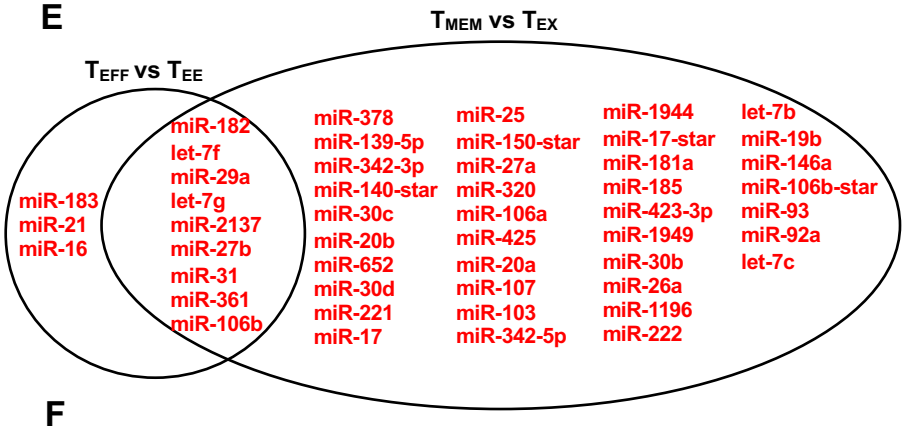

F

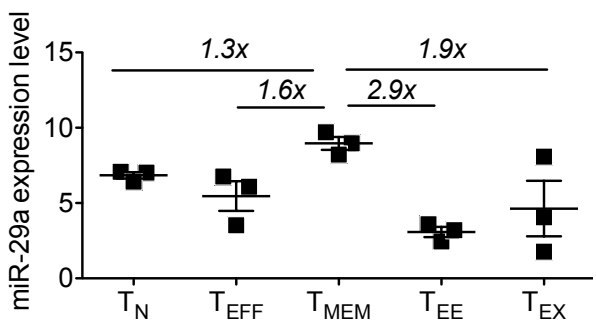

Figure S2

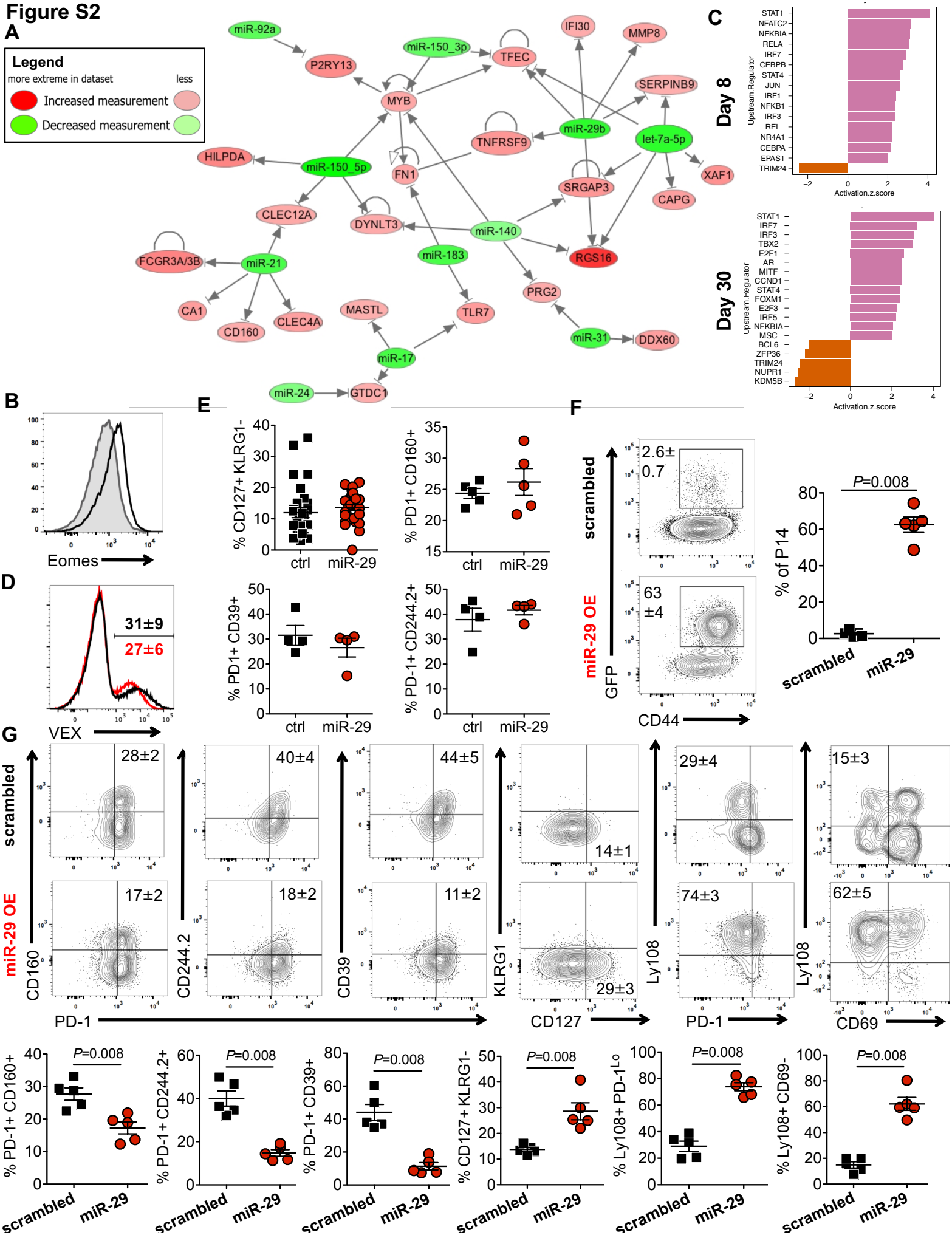
A
Legend
more extreme in dataset
less
Increased measurement
Decreased measurement
miR-92a
P2RY13
miR-150_3p
TFEC
IFI30
MMP8
MYB
SERPINB9
TNFRSF9
miR-29b
let-7a-5p
HILPDA
miR-150_5p
FN1
XAF1
SRGAP3
CAPG
CLEC12A
DYNLT3
miR-140
FCGR3A/3B
miR-21
miR-183
RGS16
PRG2
CA1
CD160
CLEC4A
MASTL
TLR7
miR-31
DDX60
miR-17
miR-24
GTDC1
C
Day 8
STAT1
NFATC2
NFKBIA
RELA
IRF7
CEBPB
STAT4
JUN
IRF1
NFKB1
IRF3
REL
NR4A1
CEBPA
EPAS1
TRIM24
Upstream.Regulator
Activation.z.score
Day 30
STAT1
IRF7
IRF3
TBX2
E2F1
AR
MITF
CCND1
STAT4
FOXM1
E2F3
IRF5
NFKBIA
MSC
BCL6
ZFP36
TRIM24
NUPR1
KDM5B
Upstream.Regulator
Activation.z.score
B
Eomes
D
31±9
27±6
VEX
E
% CD127+ KLRG1-
ctrl
miR-29
% PD1+ CD160+
% PD1+ CD39+
% PD-1+ CD244.2+
F
scrambled
miR-29 OE
2.6± 0.7
63 ±4
GFP
CD44
P=0.008
% of P14
G
scrambled
miR-29 OE
28±2
17±2
40±4
18±2
44±5
11±2
14±1
29±3
29±4
74±3
15±3
62±5
CD160
CD244.2
CD39
KLRG1
Ly108
PD-1
CD127
CD69
% PD-1+ CD160+
% PD-1+ CD244.2+
% PD-1+ CD39+
% CD127+ KLRG1-
% Ly108+ PD-1Lo
% Ly108+ CD69-
P=0.008
scrambled
miR-29

Figure S3

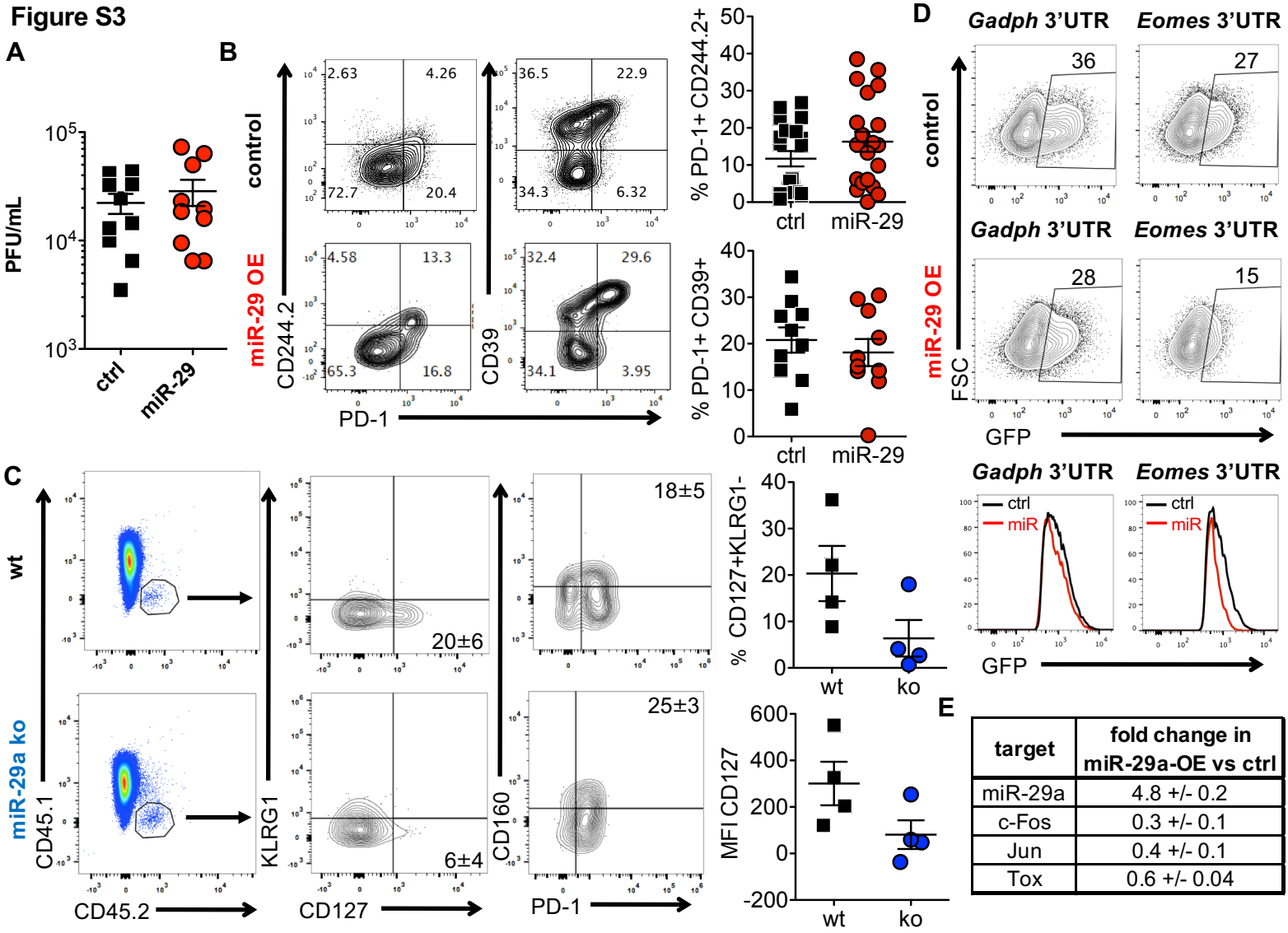

target	fold change in miR-29a-OE vs ctrl
miR-29a	4.8 +/- 0.2
c-Fos	0.3 +/- 0.1
Jun	0.4 +/- 0.1
Tox	0.6 +/- 0.04

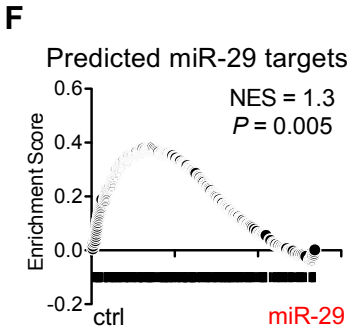

G

KLF4	ZFP36	PER1	MAT2A	TMEM132A	MEX3B	GAB1	LAMC1	DDX3X	MFSD14B	SOX12	MORF4L1
VEGFA	IFNG	MORF4L2	ASPH	INSIG1	MMP2	MFAP2	TFEB	PHC1	LIF	ELMO2	IL1RAP
FOS	WDFY3	C1QTNF6	SPTY2D1	PI15	NFIA	CTNND1	GNG12	RYBP	CMPK1	SYNE1	
COL3A1	FBN1	SRGAP3	TTYH2	PCYT1B	BCL7A	CTNNBIP1	SSC4D	PLEKHA1	YBX3	SLC31A1	
LPL	IGF1	NFIX	ZBTB47	CREB5	ADAMTS13	TDG	DCUN1D4	PTP4A1	MED12L	YPEL2	
SPRY1	BAIAP2	PMP22	SS18L1	ELOVL4	DAB2IP	HIF3A	JOSD1	MUC4	BLMH	ZFP36L1	
TMEM86A	RND3	EPB41L4B	MYCN	SNX24	CDK6	CSRNP2	SGK1	SLC1A2	TRAFD1	PER3	
ANK3	SBF2	NASP	ARRDC4	ABCB9	CHSY1	NAP1L3	ATG9A	LUZP1	MAP6	SFPQ	
RAB30	NAV1	MYBL2	MLF1	CD276	COL15A1	TNFRSF1A	ASIC1	SPPL2B	QKI	BMF	
MAFB	PDGFB	IFI30	DIO2	ENHO	CAV2	RNF19A	FAM167A	DNM3	PAIP2	VASH2	
TUBB2A	AHR	MAFG	ATP1B1	COL4A3	PEX5	NCOA4	RAPGEFL1	HECW1	EDC3	COL1A1	
BCL11A	ARRDC3	PPP1R3D	ABHD4	RND1	DUSP2	SLC16A1	HMGN3	SCML2	SYNE4	RET	
NAV2	CCDC117	MGAT4B	RASGRP4	COL16A1	AMOT	ADAM19	SH3PXD2A	TMPRSS3	PRR3	PPP2CA	

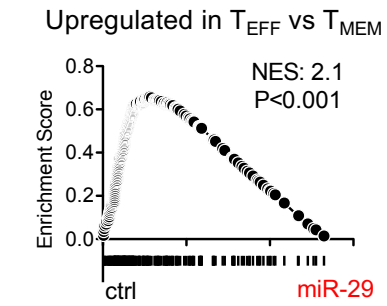

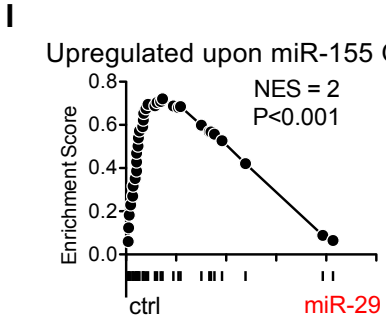

2900026A02Rik	Clspn	Gm4956
Chn2	Cd244	Med7
Cd200r1	Cd200r4	Ica1
9130019P16Rik	Cd200r2	Gm12253
Gcnt1	Cd7	Gm11992
Lrrc9	B3galt5	Pdzk1
Cela1	Slamf1	Tnfrsf9
		Grb7

Figure S4

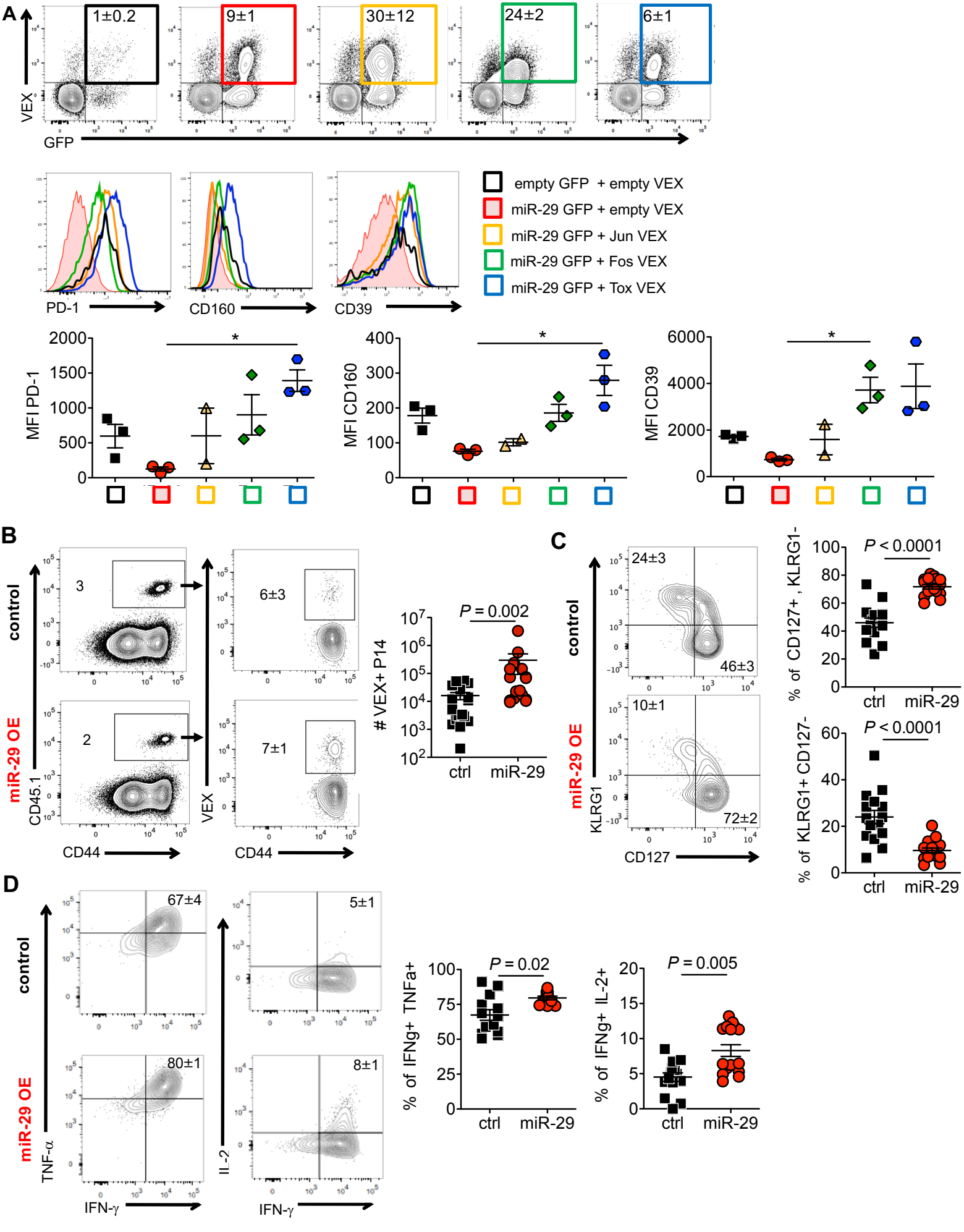
A
1±0.2
9±1
30±12
24±2
6±1
VEX
GFP
PD-1
CD160
CD39
empty GFP + empty VEX
miR-29 GFP + empty VEX
miR-29 GFP + Jun VEX
miR-29 GFP + Fos VEX
miR-29 GFP + Tox VEX
MFI PD-1
MFI CD160
MFI CD39
B
control
miR-29 OE
3
6±3
2
7±1
CD45.1
CD44
VEX
# VEX+ P14
P = 0.002
ctrl
miR-29
C
24±3
46±3
10±1
72±2
KLRG1
CD127
% of CD127+ , KLRG1-
P < 0.0001
% of KLRG1+ CD127-
D
67±4
5±1
80±1
8±1
TNF-α
IFN-γ
IL-2
% of IFNg+ TNFa+
P = 0.02
% of IFNg+ IL-2+
P = 0.005

Table S1. Differentially expressed transcripts with FDR<0.05 between ctrl and miR-29a-OE CD8 T cells.

	Gene	ID	Fold Change (log2	p-value	FDR
Upregulated in miR-29-OE versus control	Mir29a	ENSMUSG00000065610.1	1.668854047	2.24E-10	5.54E-07
	Tcf7	ENSMUSG00000000782.15	0.837606356	2.77E-07	0.00029363
	Il7r	ENSMUSG00000003882.4	1.036851526	7.02E-07	0.00057874
	Gm1070	ENSMUSG00000073018.5	1.134797738	3.87E-06	0.00239011
	Slamf6	ENSMUSG00000015314.10	0.689871863	6.12E-06	0.00349178
	Itgb1	ENSMUSG00000025809.15	0.683290415	5.94E-06	0.00349178
	Tnfrsf26	ENSMUSG00000045362.8	0.920397853	6.72E-06	0.00369158
	Gucy1a3	ENSMUSG00000033910.13	1.026657351	9.52E-06	0.00504384
	Cd8b1	ENSMUSG00000053044.8	0.689611547	1.63E-05	0.00733618
	Car12	ENSMUSG00000032373.15	0.990193713	5.26E-05	0.0199964
	Rcn3	ENSMUSG00000019539.11	0.905058776	0.00010431	0.03293237
	Slc17a9	ENSMUSG00000023393.15	0.745775601	0.00010346	0.03293237
	Smyd1	ENSMUSG00000055027.17	0.782633627	0.00011533	0.03565184
	Mypopos	ENSMUSG00000086533.2	0.747019306	0.00013306	0.03956858
	Thy1	ENSMUSG00000032011.5	0.545338348	0.00013334	0.03956858
	Nt5e	ENSMUSG00000032420.8	0.772793702	0.00018291	0.05001543
	Il18r1	ENSMUSG00000026070.15	0.617887008	0.00018539	0.05001543
Downregulated in miR-29-OE versus control	Hspa1b	ENSMUSG00000090877.3	-3.836339875	5.92E-58	8.78E-54
	Hspa1a	ENSMUSG00000091971.3	-3.612186398	3.60E-47	2.67E-43
	Hsph1	ENSMUSG00000029657.15	-2.022076315	2.84E-18	1.40E-14
	Hsp90aa1	ENSMUSG00000021270.13	-1.170705347	6.21E-18	2.30E-14
	Dnajb1	ENSMUSG00000005483.10	-1.677951352	8.83E-15	2.62E-11
	Rhob	ENSMUSG00000054364.5	-1.327772421	2.91E-10	6.17E-07
	Dnaja1	ENSMUSG00000028410.13	-1.24743132	3.52E-10	6.53E-07
	Ubc	ENSMUSG00000008348.9	-0.8749174	7.37E-10	1.21E-06
	Jun	ENSMUSG00000052684.4	-1.24247249	1.64E-09	2.44E-06
	Csf1	ENSMUSG00000014599.10	-1.360611353	4.24E-09	5.72E-06
	Gm26532	ENSMUSG00000097296.1	-1.363372744	5.34E-09	6.61E-06
	Gm37352	ENSMUSG00000103593.1	-0.996462023	2.37E-07	0.00027027
	Rgs1	ENSMUSG00000026358.13	-1.10662335	3.05E-07	0.00030129
	Tox	ENSMUSG00000041272.11	-0.788926088	3.32E-07	0.00030769
	Vcam1	ENSMUSG00000027962.14	-0.912440861	5.49E-07	0.00047892
	Slc40a1	ENSMUSG00000025993.10	-0.897654665	1.45E-06	0.00113368
	Gm26802	ENSMUSG00000097266.1	-1.242648356	2.69E-06	0.00199341
	Itgad	ENSMUSG00000070369.13	-0.908780518	3.48E-06	0.00239011
	Fos	ENSMUSG00000021250.13	-1.08225231	3.77E-06	0.00239011
	Igkv4-80	ENSMUSG00000076540.3	-1.225085692	3.65E-06	0.00239011
	Gzmk	ENSMUSG00000042385.14	-0.737611022	1.14E-05	0.00584089
	Gm8696	ENSMUSG00000092557.1	-1.075828644	1.37E-05	0.00675953
	Hspa8	ENSMUSG00000015656.17	-0.557022286	1.53E-05	0.00733176
	Klf6	ENSMUSG00000000078.6	-0.834988394	1.58E-05	0.00733176
	Gla	ENSMUSG00000031266.6	-1.008648449	1.86E-05	0.00810067
	Ccl3	ENSMUSG00000000982.5	-1.022573671	3.67E-05	0.01555889
	Klf4	ENSMUSG00000003032.8	-0.942095263	4.25E-05	0.01752651
	Morf4l2	ENSMUSG00000031422.16	-0.64176507	4.59E-05	0.01792211
	Rasgef1b	ENSMUSG00000089809.9	-1.041056627	4.59E-05	0.01792211
	Entpd1	ENSMUSG00000048120.16	-0.696113773	5.66E-05	0.02098333
	Gem	ENSMUSG00000028214.13	-0.970158208	7.06E-05	0.02493458
	Lmna	ENSMUSG00000028063.15	-1.037806404	7.03E-05	0.02493458
	Zfand2a	ENSMUSG00000053581.13	-0.988401993	7.83E-05	0.02701972
	Hspa5	ENSMUSG00000026864.13	-0.6017439	9.47E-05	0.03193246
	Hmox1	ENSMUSG00000005413.8	-0.790388106	9.96E-05	0.03285255
	Gm6297	ENSMUSG00000097123.1	-0.984276445	0.00014919	0.04340507
	Bag3	ENSMUSG00000030847.8	-0.717392403	0.00017735	0.0496501
	Selenon	ENSMUSG00000050989.9	-0.747482099	0.00017515	0.0496501
	Anxa3	ENSMUSG00000029484.12	-0.979858736	0.00019157	0.05075884
	Mrc1	ENSMUSG00000026712.3	-0.766719089	0.00019599	0.05101822
	Prdm1	ENSMUSG00000038151.13	-0.658486597	0.0002103	0.05373589
	Hdc	ENSMUSG00000027360.5	-0.974183547	0.00021367	0.05373589
	Ccl4	ENSMUSG00000018930.3	-0.919504465	0.00021933	0.05424026

Table S2. Pathway analysis reveals a role for miR-29a in regulating ribosomal pathways.

	Pathway	NES	p-value	FDR q-val
Enriched in control versus miR-29-OE	GO_HEPARIN_BINDING	1.9998995	0	9.87E-04
	GO_GLYCOSAMINOGLYCAN_BINDING	1.9728819	0	0.001476214
	GO_VIRUS_RECEPTOR_ACTIVITY	1.9051809	0	0.005832384
	GO_CARGO_RECEPTOR_ACTIVITY	1.8843999	0	0.008010143
	GO_PROTEIN_PHOSPHATASE_1_BINDING	1.8753409	0	0.006787285
	GO_CHEMOKINE_RECEPTOR_BINDING	1.8591025	0	0.007598455
	GO_CHEMOKINE_ACTIVITY	1.853316	0	0.007057953
	GO_ANTIGEN_BINDING	1.8529849	0	0.006295385
	GO_ANKYRIN_BINDING	1.8371035	0	0.007966366
	GO_PROTEIN_SERINE_THREONINE_KINASE_INHIBITOR_ACTIVITY	1.833835	0	0.007461031
	GO_INTEGRIN_BINDING	1.7880956	0	0.01530952
	GO_SULFUR_COMPOUND_BINDING	1.7853351	0	0.015010715
	GO_MHC_PROTEIN_COMPLEX_BINDING	1.7828696	0.001298701	0.014225458
	GO_CCR_CHEMOKINE_RECEPTOR_BINDING	1.7790247	0	0.014453033
	GO_G_PROTEIN_COUPLED_CHEMOATTRACTANT_RECEPTOR_ACTIVITY	1.7742513	0	0.014843537
	GO_LIPOPOLYSACCHARIDE_BINDING	1.7636839	0.002604167	0.016581804
	GO_TRANSCRIPTIONAL_ACTIVATOR_ACTIVITY_RNA_POLYMERASE_II_TRANSCRIPTION_REGULATORY_REGION_SEQUENCE_SPECIFIC_BINDING	1.7485485	0	0.019711105
	GO_CELL_ADHESION_MOLECULE_BINDING	1.7133139	0	0.034570206
	GO_SIGNALING_PATTERN_RECOGNITION_RECEPTOR_ACTIVITY	1.6940093	0.002663116	0.04318708
	GO_COLLAGEN_BINDING	1.6919171	0.001128668	0.04209192
	GO_TRANSCRIPTION_FACTOR_ACTIVITY_RNA_POLYMERASE_II_CORE_PROMOTER_PROXIMAL_REGION_SEQUENCE_SPECIFIC_BINDING	1.6858249	0	0.04437762
	GO_TRANSCRIPTIONAL_REPRESSOR_ACTIVITY_RNA_POLYMERASE_II_CORE_PROMOTER_PROXIMAL_REGION_SEQUENCE_SPECIFIC_BINDING	1.6852046	0	0.042844445
	GO_E_BOX_BINDING	1.6837938	0.002604167	0.041654456
	GO_GROWTH_FACTOR_ACTIVITY	1.6812968	0	0.041535128
	GO_ARF_GUANYL_NUCLEOTIDE_EXCHANGE_FACTOR_ACTIVITY	1.6802255	0.00249066	0.040379133
	GO_SPECTRIN_BINDING	1.6797727	0.003963012	0.03901474
	GO_SCAVENGER_RECEPTOR_ACTIVITY	1.6770134	0.002392344	0.03928865
	GO_HISTONE_DEACETYLASE_BINDING	1.6709392	0	0.041314952
	GO_CYTOKINE_RECEPTOR_ACTIVITY	1.6684775	0	0.041325763
	GO_TRANSCRIPTIONAL_ACTIVATOR_ACTIVITY_RNA_POLYMERASE_II_CORE_PROMOTER_PROXIMAL_REGION_SEQUENCE_SPECIFIC_BINDING	1.6628654	0	0.04340573
	GO_TRANSMEMBRANE_RECEPTOR_PROTEIN_KINASE_ACTIVITY	1.6586456	0.002207506	0.044135597
	GO_UNFOLDED_PROTEIN_BINDING	1.6447593	0.001059322	0.05113535
	GO_PROTEIN_LIPID_COMPLEX_BINDING	1.6384453	0.003821656	0.054071985
Enriched in miR-29-OE versus control	GO_STRUCTURAL_CONSTITUENT_OF_RIBOSOME	-2.64858	0	0
	GO_RRNA_BINDING	-2.228179	0	0.002554956
	GO_TRANSFERASE_ACTIVITY_TRANSFERRING_ONE_CARBON_GROUPS	-2.1660686	0	0.00329212
	GO_S_ADENOSYLMETHIONINE_DEPENDENT_METHYLTRANSFERASE_ACTIVITY	-2.118749	0	0.003431993
	GO_N_METHYLTRANSFERASE_ACTIVITY	-1.9876801	0	0.013086284
	GO_INTRAMOLECULAR_TRANSFERASE_ACTIVITY	-1.9746794	0	0.014042074
	GO_TRNA_BINDING	-1.9109718	0	0.021631014
	GO_RNA_METHYLTRANSFERASE_ACTIVITY	-1.8186724	0	0.046576265

Table S3. miR-29a abrogates the response to antigen signaling and inflammation.

	Pathway	NES	p-value	FDR q-val
Enriched in control versus miR-29-OE	HALLMARK_TNFA_SIGNALING_VIA_NFKB	2.2810934	0	0
	HALLMARK_INFLAMMATORY_RESPONSE	2.0561085	0	0
	HALLMARK_COAGULATION	1.9774284	0	0
	HALLMARK_ANGIOGENESIS	1.933186	0	2.55E-04
	HALLMARK_G2M_CHECKPOINT	1.8838992	0	2.04E-04
	HALLMARK_HEME_METABOLISM	1.8640239	0	1.70E-04
	HALLMARK_APOPTOSIS	1.859348	0	1.46E-04
	HALLMARK_EPITHELIAL_MESENCHYMAL_TRANSITION	1.8552928	0	1.28E-04
	HALLMARK_COMPLEMENT	1.8386849	0	1.13E-04
	HALLMARK_HYPOXIA	1.8294535	0	1.02E-04
	HALLMARK_IL6_JAK_STAT3_SIGNALING	1.8015174	0	2.75E-04
	HALLMARK_E2F_TARGETS	1.7769446	0	3.35E-04
	HALLMARK_UV_RESPONSE_UP	1.7716143	0	3.09E-04
	HALLMARK_KRAS_SIGNALING_UP	1.7480567	0	3.59E-04
	HALLMARK_TGF_BETA_SIGNALING	1.6921066	0	0.001133623
	HALLMARK_CHOLESTEROL_HOMEOSTASIS	1.6551964	0.003267974	0.001880865
	HALLMARK_IL2_STAT5_SIGNALING	1.6289208	0	0.002657183
	HALLMARK_UV_RESPONSE_DN	1.6220567	0	0.002565117
	HALLMARK_P53_PATHWAY	1.6194744	0	0.00258922
	HALLMARK_MITOTIC_SPINDLE	1.6024842	0	0.002860379
	HALLMARK_APICAL_SURFACE	1.588868	0.007083825	0.003196554
	HALLMARK_ESTROGEN_RESPONSE_LATE	1.5846844	0	0.003459575
	HALLMARK_INTERFERON_GAMMA_RESPONSE	1.5592397	0	0.004677468
	HALLMARK_ESTROGEN_RESPONSE_EARLY	1.5591127	0	0.004482574
	HALLMARK_ALLOGRAFT_REJECTION	1.5342426	0	0.006175945
	HALLMARK_APICAL_JUNCTION	1.5327951	0	0.00605468
	HALLMARK_MYOGENESIS	1.5304984	0	0.006056665
	HALLMARK_MTORC1_SIGNALING	1.482623	0	0.010572976
	HALLMARK_GLYCOLYSIS	1.4380513	0.002026343	0.017641183
	HALLMARK_PEROXISOME	1.43582	0.013948498	0.017618116
	HALLMARK_REACTIVE_OXYGEN_SPECIES_PATHWAY	1.3476757	0.06849315	0.048815593

Table S4. GSEA analysis implicates major transcription factors regulation by miR-29a.

	Pathway	NES	p-value	FDR q-val
Enriched in control versus miR-29-OE	PID_AP1_PATHWAY	2.2547114	0	0
	PID_CMYB_PATHWAY	2.1555052	0	0
	PID_FRA_PATHWAY	2.004249	0	3.54E-04
	PID_ATF2_PATHWAY	1.9475356	0	2.66E-04
	PID_NFAT_TFPATHWAY	1.908189	0	0.001312842
	PID_GMCSF_PATHWAY	1.8937105	0	0.001637884
	PID_FGF_PATHWAY	1.8743266	0	0.001875016
	PID_UPA_UPAR_PATHWAY	1.8653686	0	0.002060084
	PID_INTEGRIN3_PATHWAY	1.8543769	0	0.001831186
	PID_AURORA_B_PATHWAY	1.852264	0	0.001755662
	PID_IL23_PATHWAY	1.8099326	0	0.004490031
	PID_INTEGRIN1_PATHWAY	1.8022411	0	0.004670415
	PID_FOXM1_PATHWAY	1.7934716	0.001180638	0.004564447
	PID_INTEGRIN_A9B1_PATHWAY	1.7898757	0.001215067	0.004473784
	PID_LYSOPHOSPHOLIPID_PATHWAY	1.7629633	0	0.0069737
	PID_AVB3_OPN_PATHWAY	1.7628356	0.001177856	0.006537844
	PID_AURORA_A_PATHWAY	1.7592673	0.003558719	0.006416565
	PID_NCADHERIN_PATHWAY	1.7560147	0.00118624	0.006548575
	PID_PLK1_PATHWAY	1.7433734	0.001137656	0.007844676
	PID_AVB3_INTEGRIN_PATHWAY	1.7406168	0	0.007780236
	PID_TCR_CALCIUM_PATHWAY	1.7356753	0.002409639	0.008512248
	PID_INTEGRIN2_PATHWAY	1.6987184	0.007556675	0.013878844
	PID_INTEGRIN_A4B1_PATHWAY	1.6825811	0.003525264	0.017312404
	PID_S1P_S1P2_PATHWAY	1.6801293	0.002567394	0.016961047
	PID_FCER1_PATHWAY	1.669008	0.001091703	0.018622821
	PID_NECTIN_PATHWAY	1.647273	0.006031363	0.025575753
	PID_AJDISS_2PATHWAY	1.6435955	0.002325581	0.025613196
	PID_HIF1_TFPATHWAY	1.6431552	0.003278689	0.024815701
	PID_SYNDECAN_1_PATHWAY	1.6359407	0.002344666	0.026237834
	PID_BCR_5PATHWAY	1.6193848	0.002176279	0.03135541
	PID_PTP1B_PATHWAY	1.6159371	0.005780347	0.031833865
	PID_AR_TF_PATHWAY	1.6091808	0.005586592	0.0335987
	PID_TCPTP_PATHWAY	1.596056	0.00820633	0.03783006
	PID_E2F_PATHWAY	1.5849514	0.002190581	0.04188783
	PID_REG_GR_PATHWAY	1.582815	0	0.041841634
	PID_TOLL_ENDOGENOUS_PATHWAY	1.5810785	0.008728179	0.04174853
	PID_PI3KCI_PATHWAY	1.5708923	0.012127894	0.04646383
	PID_RET_PATHWAY	1.5676435	0.007168459	0.047392823
	PID_MET_PATHWAY	1.566764	0.001068376	0.04660435
	PID_RAC1_PATHWAY	1.5647382	0.006711409	0.046271548
	PID_IL4_2PATHWAY	1.5534688	0.011866235	0.05104758